RAPID RECONNAISSANCE AND RESPONSE (R^3)

MISSION PLAN

by

Jenny Kelly, Mission System Engineer
David Spencer, Principal Investigator

Documentation to support the mission design and operations of:

R^3 Mission
Center for Space Systems
Georgia Institute of Technology

April 2010

Approved by ____

Date ____

REVISIONS

Revision	Description	Date	Approval
___	Initial Release	2/14/10	
A	Team Lead Edits, CDR changes	4/30/10	

TABLE OF CONTENTS

LIST OF FIGURES

LIST OF TABLES

NOMENCLATURE

ADCS	Attitude Determination and Control Subsystem
ACS	Attitude Control Subsystem
ADS	Attitude Determination Subsystem
AFRL	Air Force Research Laboratory
BPSK	Binary Phase Shift Keying
C&DH	Command and Data Handling
CCD	Charge-Coupled Device
DIME-1	Dosimetry Intercomparison and Miniaturization Experiment 1
DSP	Digital Signal Processor
EPROM	Erasable Programmable Read-Only Memory
EPS	Electrical Power Subsystem
FBSC	Full Battery State of Charge
FCR	Flight Competition Review
FSW	Flight Software
FPGA	Field-Programmable Gate Array
GMSK	Gaussian Minimum Shift Keying
GPS	Global Positioning System
IC	Integrated Circuits
ISS	International Space Station
JPL	Jet Propulsion Laboratory
JTAG	Joint Test Action Group
LBSC	Low Battery State of Charge
LEO	Low Earth Orbit
LHC	Left-Hand-Circular
LNA	Low-Noise Amplifier
ODS	Orbit Determination Subsystem
POST II	Program to Optimize Simulated Trajectories
R^3	Rapid Reconnaissance and Response
RADFET	Radiation-Sensing Field-Effect Transistor
RF	Radio Frequency
RHC	Right-Hand-Circular
SEL	Single Event Lockup
SEU	Single Event Upset
SPI	Serial Peripheral Interface
SSTL	Surrey Satellite Technology Limited Inc.
STK	Satellite Tool Kit
TTL	Transistor-Transistor Logic
UNP	University Nanosat Program
UVPROM	Ultra-Violet Programmable Read-Only Memory

INTRODUCTION

The Rapid Reconnaissance and Response (R^3) Mission Plan defines the baseline mission and discusses the set of activities for which spacecraft sequences and ground procedures will be developed and tested. The Mission Overview section summarizes the mission and its objectives, as well as the mission phases and spacecraft modes defined for the project. The Flight System section describes the baseline satellite subsystems, while the Instruments section discusses the radiation dosimeter, microbolometer, and visible imager that will be used for science operations. Finally, the Mission Design section describes the image processing algorithms to be used onboard the spacecraft, along with certain analyses that were performed to support the design of the mission. This document will be updated periodically to reflect the current state of the mission design and operations plan. In addition, the information in this document supersedes the information contained in the following memos: R3-TM-2009-013 and R3-TM-2010-001 (Orbit Analysis); R3-TM-2010-002 (Data Return Strategy); and R3-TM-2009-017 and R3-TM-2010-03 (Mission Phases and Spacecraft Modes of Operation).

MISSION OVERVIEW

MISSION SUMMARY

The Rapid Reconnaissance and Response (R^3) mission will characterize the radiation environment effects on an uncooled microbolometer thermal imager, perform thermal and visible imaging from low Earth orbit, and demonstrate the autonomous detection and geolocation of thermal features using onboard image processing algorithms. The entire process from satellite image acquisition to transmission of thermal feature coordinates to the ground will be fully automated. A visible camera will provide context for the thermal images, and a radiation dosimeter will measure the satellite's radiation environment. A six-month mission will test the onboard image processing algorithms against a diverse range of thermal features and allow the R^3 team to characterize the effects of radiation on the performance of the microbolometer.

The R^3 satellite will demonstrate autonomous detection and geolocation of thermal features by identifying coastal currents, coastal eddies, and ocean gyres. Ocean currents can be identified based upon surface temperature differentials with the surrounding waters. The currents may be broadly distributed, as they are for large ocean circulation features such as the Gulf Stream, or localized, as they are for river outflows and shoreline-generated eddies. Identification of these features is useful for the validation of current modeling and long-term weather forecasting. In addition, the rapid geolocation of coastal currents will benefit the oceanographic science community in the planning of cruises for collection of in-situ observations. Monitoring of ocean currents also has direct application to the energy efficiency of maritime operations, as shipping routes can be optimized to take advantage of favorable time-varying currents.

The student-built R^3 satellite is based upon a straightforward system design with robust operating margins. In addition, use of an uncooled microbolometer instead of a more traditional cryogenically cooled thermal imager will result in significant mass and power savings and allow for rapid integration with the flight system. Thus, the mission will be accomplished on a budget and schedule that represent a small fraction of the resources that such a mission would require if developed within the Department of Defense or the aerospace industry.

The R^3 satellite will be launched as a secondary payload on a launch vehicle to be identified following the selection of the University Nanosat Program (UNP) mission. The orbit that R^3 satellite may be delivered into by the primary payload's launch system is highly variable. The R^3 mission is designed to be robust to a range of operational orbits. Orbit altitudes of 300-600 km can be accommodated, with a corresponding decrease in thermal image spatial resolution at the higher altitudes. The R^3 team has compiled an array of candidate thermal features, allowing the selection of features tailored to the satellite's viewing geometry.

Following separation from the launch vehicle, the R^3 attitude determination and control system will damp attitude rates using magnetic torquers and perform initial attitude determination using a magnetometer. The S-band transceiver will begin to transmit a radio frequency (RF) signal, which will be acquired by the Center for Space Systems ground tracking station at Georgia Tech. The Georgia Tech tracking station will be utilized for both R^3 satellite commanding and data return; additional university tracking stations may be utilized for data downlink as necessary based upon viewing geometry. Early tracking data will allow the determination of the R^3 satellite orbit parameters. An orbit ephemeris will be developed, and view periods for imaging and communication will be established. Normal operations will proceed for the duration of the six-month mission.

MISSION OBJECTIVES

The primary objectives of the Rapid Reconnaissance and Response (R^3) mission are to characterize the radiation environment effects on an uncooled microbolometer thermal imager, to perform thermal and visible imaging from low Earth orbit, and to demonstrate onboard thermal feature detection and geolocation.

To achieve these objectives, the R^3 satellite will acquire thermal images of specified regions on the surface of Earth using an uncooled microbolometer. Onboard image processing algorithms will detect and identify coastal currents, coastal eddies, and ocean gyres within the thermal images. The coordinates (latitude and longitude) of the thermal features will be computed onboard and downlinked to the R^3 team. The R^3 satellite will also use a visible camera to acquire visible images of the feature and surrounding area, which will provide context for the thermal images. In addition, a radiation dosimeter onboard the R^3 satellite will measure the radiation environment surrounding the satellite. The R^3 team will use the radiation total dose and single event data to assess the effect of radiation on the performance of the uncooled microbolometer.

The R^3 mission duration will be six months or longer, with an orbit altitude between 300 and 600 km (the lower altitude limit is constrained by the minimum mission duration required to collect sufficient radiation data, while the upper limit is constrained by the maximum allowable time to deorbit, which is 25 years). The mission will provide educational outreach opportunities and fulfill two technology areas of interest to the Air Force: radiation environment effects and advanced electro-optical sensors, as listed in Appendix B of the Nanosat-6 User's Guide.

MISSION PHASES & SPACECRAFT MODES

The overall R^3 mission is divided into smaller time periods known as mission phases, and a set of ground procedures is associated with each phase. Mission phases are distinct from spacecraft modes, which are the different states of operational capability in which the satellite can function. Thus, the satellite may operate in more than one mode (though not simultaneously) over the duration of a mission phase. Since the spacecraft modes are programmed into the satellite's onboard computer before launch, the sequences for each mode must be executed autonomously, but the spacecraft can also receive and execute commands from the ground. Seven mission phases and three spacecraft modes are used to describe the periods of satellite and ground station activity during the R^3 mission.

Mission Phases

The mission phases defined for the R^3 mission are listed in Table 1 and described in detail in the following sections.

Table 1. Definition of R^3 mission phases.

Phase	**Start of Phase**	**End of Phase**	**Length**
Launch	Terminal countdown	Separation from launch vehicle	TBD
Startup	Separation from launch vehicle	Flight computer boots	< 5 min
Initial Acquisition	Flight computer boots	Health & status check complete	5-56 hrs
Checkout	Health & status check complete	Checkout complete	~1 week
Normal Operations	Checkout complete	End of 6-month science mission	6 months
Extended Mission	End of 6-month science mission	End of usable life	TBD
End of Mission	End of usable life	Disposal	TBD

Launch

The launch phase extends from the initiation of the terminal countdown to separation of the R^3 satellite from the launch vehicle. The launch vehicle, location, and opportunities are currently unknown, as is the orbit into which the satellite will be injected. Launch details will become available no earlier than the selection of the flight nanosat at the Flight Competition Review (FCR) in January 2011.

Startup

The startup phase begins with separation of the R^3 satellite from the launch vehicle and ends when the flight computer has completed its startup sequence. During this time, ground control will monitor Air Force tracking of the satellite and update estimates of expected tracking station overflight times. The satellite will remain in startup mode (defined in a later section) for the duration of the phase.

Initial Acquisition

The initial acquisition phase extends from the time the flight computer completes its startup sequence until an initial health and status check is complete. Ground control will establish telemetry-only communication with the satellite at a low data rate (to maximize signal strength), and the R^3 team will use the telemetry to evaluate the health and status of the satellite. The satellite will remain in safe mode (defined in a later section) for the duration of the phase.

Checkout

The checkout phase begins when the initial health and status check is complete and ends when spacecraft subsystems have been tested for nominal operating performance. While the satellite remains in safe mode, the R^3 team will test selected subsystems for nominal operating performance. The tests currently planned for safe mode are as follows:

- Telecommunications: data rate tests
- Flight Software: diagnostic tests

Safe mode will then be exited through ground command and the satellite will proceed through the ground-in-the-loop safe mode exit sequence, slewing to the imaging attitude and establishing two-way communication with the ground at a nominal data rate. The remaining tests will be performed with the satellite in normal mode:

- Attitude Determination & Control: reaction wheel desaturation
- Science Instruments: sensor calibration and tests
- Thermal: heater tests

Normal Operations

The normal operations phase extends from the completion of checkout to the end of the six-month baseline science mission. Throughout this phase, images, radiation data, and telemetry will be returned to the ground during each overflight of the Georgia Tech tracking station. In addition, the R^3 team will conduct a weekly mission planning process. The most recent orbital state of the satellite will be propagated forward for two weeks, and the satellite's ground track will be compared to seasonal Gulf Stream data to select specific imaging opportunities. The R^3 team will then compile two flight tables to be uploaded to the satellite: one of the selected imaging opportunities, and another of expected overflight times of the Georgia Tech tracking station.

Extended Mission

When the baseline science mission is complete, satellite operations will continue in an extended mission phase until the end of the satellite's usable life. During this phase, the satellite will continue acquiring science data until the science instruments are no longer operable. Control of the satellite will then be transferred to amateur radio operators for an agreed-upon period of time. The end of the amateur radio operation period will define the end of the satellite's usable life, unless it is preceded by a critical component failure or the satellite reaching 200 km altitude.

End of Mission

The end of mission phase extends from the end of the satellite's usable life until its disposal, which occurs when the satellite reaches 78 km altitude and burns up in the Earth's atmosphere. During this phase, ground control will execute a series of commands to perform end-of-mission safing of the R^3 satellite. These commands will include turning off radio transmission, disconnecting batteries from the system, and shorting batteries and solar arrays to shunt resistors.

Spacecraft Modes

The three spacecraft modes defined for the R^3 mission are listed below and described in detail in the following sections.

- Startup Mode
- Safe Mode
- Normal Mode

Startup Mode

Once the satellite enters sunlight, the Command and Data Handling (C&DH) subsystem will activate and begin charging the battery. The satellite will autonomously initiate the startup sequence on the flight computer, which includes monitoring the battery state of charge, initiating thermal control, activating the telecom transceiver (receive only), and initiating the recording of telemetry from subsystems. Upon completion of the startup sequence, the satellite will change the mission phase bit to safe mode.

Transitioning to Safe Mode

The satellite can enter safe mode in three primary ways: (1) after the battery is initially charged during startup, (2) upon receiving a command from ground, or (3) after anomalous behavior. Potential anomalous behaviors have been identified and include: deviations from predicted performance, loss of attitude/position knowledge, loss of attitude control, unexpected loss of communication with ground, and subsystems reaching a critical point (e.g., computer is reset, battery reaches maximum depth-of-discharge, electrical fault, loss of power production for a period longer than the maximum expected eclipse time, etc.).

Safe Mode

Upon entering safe mode, the satellite will perform two sequences of autonomous tasks: a low battery state of charge (LBSC) sequence followed by a full battery state of charge (FBSC) sequence. During the LBSC sequence, any other active sequences will be terminated and the statuses of specific spacecraft components will be asserted as shown in Table 2. The flight computer will then monitor the battery state of charge.

Table 2. Component statuses asserted during the safe mode LBSC sequence.

Component	**Status**
Science instruments	OFF
Reaction wheels	OFF
Star tracker	OFF
C&DH subsystem	ON
Telecom transceiver (receive)	ON
Telecom transceiver (transmit)	OFF
Magnetometer	OFF
Torque rods (phased with magnetometer)	OFF
GPS	OFF

Thermal heaters	ON

When the previous sequence is complete and the battery is fully charged, the FBSC sequence will be initiated. Coarse attitude determination and control will be activated by asserting component statuses as shown in the first three rows of Table 3. The satellite will then execute its detumble procedure, damping any spin rates with the magnetic torquers. The telecom transmitter will be powered ON/OFF via an overflight table onboard the satellite (i.e., the transmitter will only be ON during overflights of the Georgia Tech tracking station), also reflected in Table 3. Telemetry-only communication with the ground will be established at a low data rate to maximize signal strength.

Table 3. Component statuses asserted during the safe mode FBSC sequence.

Component	**Status**
Magnetometer	ON
Torque rods (phased with magnetometer)	ON
GPS	ON
Telecom transceiver (transmit)	ON/OFF via overflight table

Exiting Safe Mode

When both the LBSC and FBSC safe mode sequences are complete, the satellite can transition to normal mode in one of two ways: autonomously or ground-in-the-loop.

If the safe mode entry was due to exceeding the maximum battery depth-of-discharge, safe mode can be exited through an autonomous exit sequence. By allowing the satellite to respond autonomously, the R^3 team avoids wasting several days of operation on a relatively straightforward problem. The exit sequence will begin with the satellite transitioning to fine attitude determination and control, asserting component statuses as shown in the first four rows of Table 4. The satellite will then prepare for normal operations by orienting for imaging; the imaging attitude is nadir-pointing, with the imager's vertical field of view aligned with the velocity direction. Finally, the satellite will establish two-way communication with the ground at a normal data rate, initiate the imaging sequence, and change the mission phase bit to normal mode.

Table 4. Component statuses asserted during the autonomous safe mode exit sequence.

Component	**Status**
Reaction wheels	ON
Star tracker	ON
Magnetometer	OFF
Torque rods (phased with magnetometer)	OFF
Science instruments	ON

If the safe mode entry occurred for any other reason than exceeding the maximum battery depth-of-discharge, a ground-in-the-loop exit sequence must be used. This exit sequence will be a prepared contingency plan response with different paths for different causes of safe mode entry.

Normal Mode

Upon entering normal mode, the satellite will initiate normal operations. This includes acquiring thermal and visible images of specified regions via sequenced commands from ground control, detecting and geolocating thermal features, and measuring the radiation environment surrounding the microbolometer.

Summary of Phases & Modes

Figure 1 shows a flow chart depicting the satellite's progression through each of the post-launch mission phases. The corresponding spacecraft modes of operation appear adjacent to each phase.

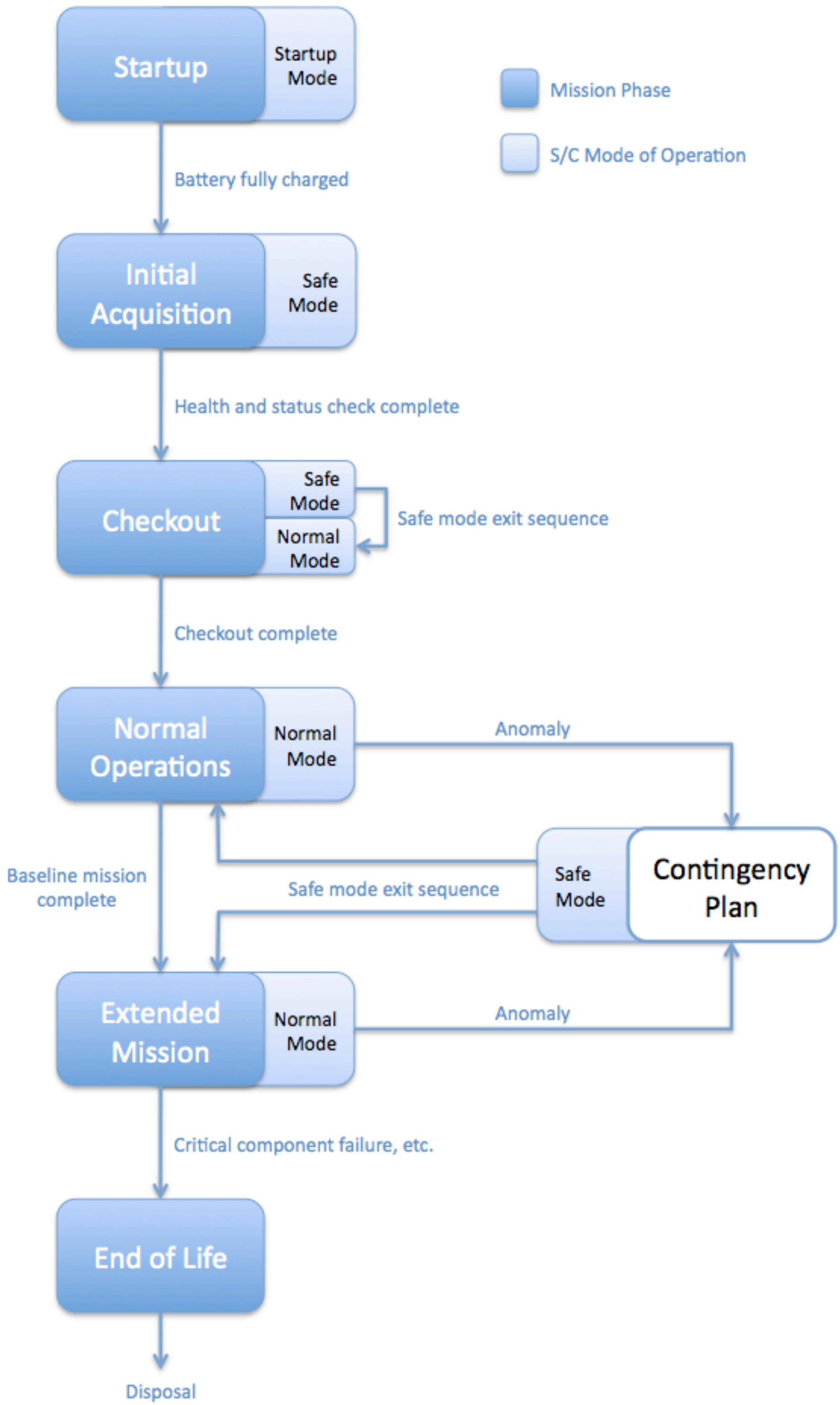

Figure 1. Flow chart summarizing mission phases and spacecraft modes.

TRACKING REQUIREMENTS

Tracking coverage of the R^3 satellite by the Georgia Tech ground station (33.78°N, -84.40°W) will be achieved using a dish antenna with a gain of 30 dB and a 20° elevation mask. A low noise amplifier with a gain of 21 dB will be used to improve the satellite's data volume downlink capability. Coverage by additional ground stations at lower latitudes may be made possible at a later date.

The tracking requirements depend on the satellite's orbit, which is not known at this time. However, the average parameters across all orbits being considered are 2.7 passes/day, with an average pass duration of 3.8 min/pass.

FLIGHT SYSTEM

ATTITUDE DETERMINATION AND CONTROL SUBSYSTEM

The attitude determination and control subsystem (ADCS) is comprised of a several smaller subsystems: the attitude determination subsystem (ADS), the attitude control subsystem (ACS), and the orbit determination subsystem (ODS). Furthermore, both the ADS and the ACS are broken into fine and coarse capabilities.

The coarse ADS will be used during safe mode and consists of a magnetometer. The baseline magnetometer is the TFM65-VQS, produced by Billingsley Aerospace & Defense. Since the magnetometer will be used periodically but not constantly, a Kalman filter will take in the most recent measured magnetic field vector to predict the spacecraft attitude between magnetometer readings.

The fine ADS will be used during normal operations and consists of a star tracker. The star tracker produces an inertial quaternion, essentially providing the attitude with minimum analysis. The selected star tracker is a Star Tracker ST purchased from Valley Forge Composite Technologies.

Like the coarse ADS, the coarse ACS will be used during safe mode. It consists of three torque rods, placed such that three axes can be controlled. The torque rods will react with the Earth's magnetic field to adjust the attitude of the satellite. The torque rods will be designed and fabricated in-house. The current design baselines for the torque rods to provide up to a 10 Am^2 linear dipole moment, which is sufficient for controlling the attitude of the R^3 satellite.

The fine ACS consists of three reaction wheels, one for each axis. The baseline reaction wheels are the 0.1 N-m-s wheels produced by Valley Forge Composite Technologies. Like all reaction wheels, these wheels are subject to saturation; therefore, the torque rods, used primarily in the coarse ACS, will also be used to desaturate the fine ACS components.

A Global Positioning System (GPS) unit will provide orbit determination. The baseline unit is the SGR-05U, which is sold by Surrey Satellite Technology Ltd. This unit will provide position, velocity, orbital elements, and time.

TELECOMMUNICATIONS SUBSYSTEM

The primary goal of the R^3 telecommunications (telecom) subsystem is to provide uplink and downlink of all mission data, telemetry, and commands between the R^3 satellite and the ground station. This link must be reliable for the duration of the communications window, which was calculated to vary between approximately 2.4 and 5.5 minutes, depending on the spacecraft's orbit. The onboard communications components consist of an S-band circular antenna, UHF monopole antenna, S-band transmitter, UHF receiver, and connective wiring, resulting in a total mass of less than 0.5 kg. The system will use Binary Phase Shift Keying (BPSK) as the form of data modulation, and the antenna can be polarized to Left-Hand-Circular (LHC) or Right-Hand-Circular (RHC). This configuration will provide sufficient data rates for the communications system while limiting power consumption.

The R^3 mission will operate within the amateur S-band frequency range for downlink, allowing for the use of a high data rate (up to 1 Mbps) necessary to meet mission data volume requirements. This frequency range also creates a reliable communication link that is less susceptible to wavelength interference than lower frequencies. The uplink will operate within the amateur UHF frequencies at a data rate of 9600 baud, which corresponds to the limiting factors of the ground station hardware.

All hardware for this subsystem will be provided by Space Quest Incorporated. The S-band antenna selected is the AC-100 Circular Antenna, which will provide sufficient gain for downlink and a very wide (160°) beam width. The UHF antenna will be the ANT-100 monopole antenna, which will provide sufficient gain for the low data rate uplink. The R^3 satellite will also use a TX-2400 S-band transmitter, capable of operating at data rates of up to 1 Mbps and supporting 2.5 W of RF power at 800 mA. The receiver will be the RX-445 UHF receiver, which is the size of a matchbox, weighs 40 g, and is capable of 9600 bps working with Gaussian Minimum Shift Keying (GMSK) modulation. All components selected for the telecommunications subsystem have a long flight heritage, low mass and cost, and small volume.

ELECTRICAL POWER SUBSYSTEM

The electrical power subsystem (EPS) will generate, store, and distribute power during the R^3 mission. Ultra triple-junction solar panels with a total surface area of 0.98 m^2 are body-mounted on the four side panels of the satellite. There are a total of 360 cells, connected in 24 strings of 15 cells each. During an optimal orbit, these panels are capable of producing a time-averaged power of 145 W. During the worst-case orbit, the panels produce 80 W, and the expected value (the mean power production across all orbits) is 95 W per orbit. This production rate allows the satellite to charge the battery while providing sufficient power margin, since the satellite requires 49 W for nominal operation during one orbit.

The EPS also regulates voltage and distributes power to the other subsystems. Separate internal regulators buck the bus voltage for each subsystem. The EPS uses a Sun-regulated direct energy transfer architecture for power distribution. Non-critical flight loads are fused, and switches are placed upstream of the regulator where possible to conserve power when the regulator is not in use. A mode controller will ensure that the proper flight loads are switched on to comply with the desired operational modes of the spacecraft.

A stand-alone battery charge regulator will regulate charging of the battery during daylight; excess power will be bled-off via a resistive shunt. The battery charge regulator is capable of fast- and trickle-charging the batteries. The charge controller will ensure that the batteries do not overheat during charging. During eclipse, power will be supplied by a 24-cell Nickel Cadmium (Ni-Cd) battery pack. The batteries are capable of reaching a depth of discharge of 40% and still lasting the life of the mission, including sufficient margin.

The spacecraft bus will be powered directly via the solar panels and batteries. To prevent operation before the satellite is a safe distance away from the launch vehicle, three magnetic inhibits on the high side and one on the low side of the batteries will prevent turn on before the flight computer deems it acceptable. Another set of inhibits, called light band separation switches, will be located between the solar panels and the spacecraft loads in a similar configuration to the battery inhibits. When the satellite detaches from the launch vehicle, the light band switches will close and allow the solar panels to supply power to the flight loads.

STRUCTURES SUBSYSTEM

The structure of the R^3 satellite is designed entirely out of aluminum (Al 6061-T6) to reduce weight and cost. The structure forms a 46 x 46 x 57 cm rectangular prism, which provides adequate margin in each direction to accommodate external instruments such as solar panels or antennas and still remain within the volumetric constraints of the program. To remove as much excess weight as possible, each side of the satellite will feature triangular patterned cutouts, leaving enough material to maintain structural integrity and properly mount all equipment. All instruments will be mounted directly to the faces to minimize internal structure and create a simple and stable final assembly. The visible camera, microbolometer, and patch antenna will be mounted on the nadir face, while the launch vehicle interface ring will dominate the zenith face. Solar panels will be lofted from the side faces to isolate them from the thermal deformation of the aluminum plates and keep the solar panel substrate from bearing a load. The star tracker will be mounted on a chamfered corner with attention paid to avoiding any light contamination from the Earth or from the satellite itself.

Finite-element analysis of the structure will show that it can withstand expected launch loadings of approximately 20 g's. Similarly, modal analysis will show that the structure's natural frequency avoids any expected launch frequencies.

Launch Interface

Since the R^3 satellite will be a secondary payload, it must separate with as little disturbance to the launch vehicle as possible. A non-pyrotechnic separation system is desirable. The University Nanosat Program provides each flight satellite with a Mark II motorized Lightband launch separation system, produced by Planetary Systems Corporation.

The Lightband is a non-pyrotechnic, low shock, motorized clamp band. One ring is bolted to the satellite body using 24 attachment points. The other ring is bolted to launch vehicle interface and includes the motor and separation springs. The two rings are then compressed together and the clamps are engaged. On orbit, the motor engages and releases the clamps, allowing the separation springs to release and gently push the satellite away from the launch vehicle. On the R^3 satellite, the satellite-side ring is mounted to the zenith-facing plate and thus does not interfere with the science instruments.

The provided Lightband is 38.1 cm (15 inches) in diameter, as is the corresponding bolt-hole pattern on the satellite body. In its stowed configuration, the Lightband is approximately 5.3 cm (2.1 inches) tall. The assembly will extend outside the satellite envelope.

THERMAL CONTROL SUBSYSTEM

The primary requirement of the thermal control subsystem is to maintain all spacecraft components and hardware within their operational and survivable temperature ranges during all phases of the mission, excluding end-of-mission disposal. This will be accomplished using as much passive control as possible. In circumstances where specific components require more stringent thermal control, active mechanisms will be employed. Passive devices are preferred because of the risk and complexity associated with active devices, but the need for each type of thermal control will be determined through thermal modeling and analysis.

Thermal analysis of the R^3 satellite will be conducted on three separate finite differencing models: single-node, six-node, and detailed. The first two analyses have been completed, and the detailed analysis is currently in progress. Heating conditions included in each of the analyses were direct solar, albedo, Earth IR, and both internal and external radiative and conductive heating.

The first and simplest model consisted of a single node, assuming the satellite to be a sphere to give a basic understanding of the range of temperatures experienced by the spacecraft. A second model, created in MATLAB, consisted of six nodes, with each node representing a face of the spacecraft and all attached components. The model was run for four different environmental heating cases: worst-case hot on-orbit, worst-case cold on-orbit, safe mode, and pre-startup. An identical six-node model was created in Thermal Desktop and was used to validate the outputs of the finite differencing code. Based on the hottest and coldest temperatures experienced by each face of the spacecraft, all components require some form of thermal control except for the solar cells, magnetic latching, and voltage converter. Most of the components can be passively maintained within their operational and survivable temperature ranges by applying thermal coatings, multi-layer insulation, and intelligent packaging methods. For components that require additional heating, small resistive heaters will provide active thermal control.

The final model represents the satellite on an individual component level and was created using Thermal Desktop, a SINDA/FLUINT solver. The detailed model allows for each component to be thermally analyzed within the expected environments, and thermal control devices such as insulation, coatings, and heaters can be added to determine their effects. Upon completion of the detailed thermal analysis, the type and quantity of thermal control components will be determined, taking the current hardware and packaging into consideration. Associated risks and mitigation strategies will be analyzed after component selection.

COMMAND AND DATA HANDLING SUBSYSTEM

The command and data handling (C&DH) subsystem is responsible for all the computational aspects of the spacecraft, including command and telemetry handling, power monitoring and management, thermal monitoring and management, payload image processing, and attitude determination and control. The C&DH subsystem is composed primarily of a floating-point

Digital Signal Processor/Field-Programmable Gate Array (DSP/FPGA) combination processor board and a power/sensor board.

The processor board contains two 128-megabyte volatile memory banks (one for the DSP and one for the FPGA) and 256 megabytes of nonvolatile memory. The DSP will run the flight software and perform the image processing, while the FPGA will process the interface logic for subsystems external to the C&DH subsystem. These external subsystems are connected through the interface electronics on the power/sensor board. Communication between the DSP and the FPGA is facilitated by a high-speed internal data bus.

The power/sensor board takes power from the EPS and converts it to the proper voltages for the rest of the C&DH components. This board includes all the physical interfaces that connect to the rest of the spacecraft. RS422 data buses are used to interface with the GPS, star tracker, and transceiver. A Serial Peripheral Interface (SPI) bus is used to communicate with the multiplexed analog to digital converter (to which all analog inputs are connected). An IEEE1394a bus interfaces with the visible camera, while a standard camera interface is used to interface with the microbolometer. Transistor-Transistor Logic (TTL) will be used to connect the reaction wheels and torque rods to the C&DH subsystem.

The nonvolatile memory will utilize triple modular redundancy, since it will be temporarily storing mission data in addition to operation data and since the volatile memory will be scrubbed by the FPGA. The Joint Test Action Group (JTAG) interface to the DSP will be accessible to the FPGA for Single Event Upset (SEU) and Single Event Lockup (SEL) mitigation. The C&DH electronics will be encased in a 7.62 mm thick aluminum case to reduce electromagnetic interference and radiation effects. An additional thin layer of tantalum will be used to provide additional radiation protection.

The C&DH subsystem will be connected to a host computer for development and debugging purposes through a JTAG port connected to the DSP. A JTAG emulator will enable the host to communicate with the C&DH subsystem via a USB port and allow for code uploading as well as debugging features such as printouts and break points.

FLIGHT SOFTWARE SUBSYSTEM

The R^3 satellite's flight subsystems are connected to and controlled by the C&DH subsystem, which will run customized flight software (FSW). The flight software will be written in a modular manner using the C/C++ languages and will contain a persistent operating system embedded on the C&DH subsystem. Separate tasks will be switched in the same manner as processes or threads are switched on common personal computers. Tasks are contained within separate modules designed for modularity and reuse.

The modules will receive commands and action sequences from mission control via the telecommunications subsystem. These commands will be translated into predetermined spacecraft actions and operating signals, which will be programmed before launch. The operating signals will be concurrent sequences that will perform blocking on the required components in a prioritized closed-system manner. This design will allow the flight software to run multiple tasks while concurrently accepting and executing new commands and sending requested telemetry and science data.

The concurrent collection and distribution of data will be mediated by a central data repository with select meta-data. Data will be gathered from the science and engineering devices and versioned into memory with time and date stamps for future reference. The lifespan, downlinked priority, and importance of all data can be modified and controlled via ground command, but default values will be given to enable autonomous operation. Ground control of these parameters can be as fine-tuned as selecting individual data sets or can be generalized to threshold filtering and selecting of data.

The flight software is also required to control specific subsystem functionality. Two examples of this are the attitude control subsystem, which requires control functions to analyze and respond to environmental variables, and the electrical power subsystem, which requires a monitoring and management function to respond to internal constraints and levels.

Finally, the flight software is responsible for fault protection, which involves frequent overall health checks of the satellite to determine if a problem has occurred. If the flight software senses a problem, it will automatically execute a series of preset functions to reach a resolution. In more extreme cases, the flight software can detect that certain actions, such as communication with the ground, have not been performed for extended period of time. The software can then respond on a preset time delay in the case of total failure. In the case of complete failover, the flight software operates in a separate mode with minimal functionality, allowing problems to be diagnosed via ground analysis of onboard telemetry.

SCIENCE INSTRUMENTS

RADIATION DOSIMETER

The R^3 satellite will use a radiation dosimeter to quantify the radiation environment surrounding an uncooled microbolometer, and the resulting data will be used to assess the effect of radiation on the microbolometer's performance. The dosimeter selected for the R^3 spacecraft is the Dosimetry Intercomparison and Miniaturization Experiment 1 (DIME-1).

DIME-1 was designed by Clemson University under the direction of Dr. Peter McNulty. DIME-1 is a small (10 x 15 cm) circuit board printed with a variety of integrated circuits (IC's) to perform radiation dosimetry. There are two types of dosimeters used on the DIME-1. Three Ultra-Violet Programmable Read-Only Memory (UVPROM) units will measure the total dosage of ultra-violet radiation, as well as provide a quantification of Single Event Upsets (SEU). The UVPROM units are affected by various types of radiation, from large proton radiation to much smaller radiation types. In addition, six Radiation-Sensing Field-Effect Transistor (RADFET) units will be used with varying levels of shielding to provide calibration of shielding effects. DIME-1 also possesses a small microprocessor for handling and manipulating data before passing it on to the central processor. The dosimeter flies in an unpowered state for large periods of time, only powering on periodically to read the memory IC's to update the total dose and SEU data. In its powered state, DIME-1 uses less than one watt of power. The dosimeter will be situated close to the microbolometer in order to most accurately measure the radiation environment that the microbolometer experiences.

MICROBOLOMETER

The R^3 satellite will use a microbolometer to produce thermal images, which will be used in conjunction with image processing algorithms to accomplish thermal feature detection. The use of an uncooled microbolometer instead of a more traditional cryogenically cooled thermal imager will result in significant mass savings and allow for rapid integration with the flight system.

The microbolometer consists of a 640 x 480 array of thermal sensor elements. Incoming light with wavelengths of about 8-13 μm will excite the thermal sensors, causing a change in their resistance. The potential differences across the sensors will then be measured and converted to a temperature corresponding to the emission of the measured electromagnetic energy. Raytheon Vision Systems will supply the microbolometer array and readout electronics as part of a UE460 camera engine. The camera engine will output a digital signal of the potential differences measured by the array element.

The array and camera engine system will be fastened to a machined coupler that will attach to an infrared lens. The baseline lens is a manual focus Ophir SupIR f/1 100 mm lens (model number 65040), which will be focused to infinity. The lens has a primary diameter of 10 cm, resulting in a diffraction limit of 34 arcseconds for radiation at 13.6 μm. Combined with the microbolometer, it will give a field of view of 9.1° x 6.8° (crosstrack by downtrack), with a pixel width (instantaneous field of view) of 51 arcseconds.

The R^3 team calculated the expected amount of pixel smearing, a blurring effect due to the slight shift in image footprint during the time necessary to acquire an image. At an altitude of 500 km, the image footprint will be 79 x 60 km, giving each pixel a width of 124 m. The microbolometer has a thermal time constant of less than 0.016 s. In that time and at an altitude of 500 km, the image footprint will move downtrack by 0.9 pixels, causing slight pixel smearing. At higher altitudes, the image footprint will be larger, resulting in coarser resolution but less pixel smearing.

VISIBLE IMAGER

The R^3 satellite will use a visible camera to image specified regions on the surface of the Earth, and the resulting visible images will be used to provide context for the thermal images obtained from the microbolometer. The camera selected for this task is the Grasshopper (model GRAS-

14S3C) manufactured by Point Grey Research Inc. This is a 1.4-megapixel camera with a 1384 x 1032 CCD (Charge-Coupled Device) array.

The camera lens was selected to give the best overall performance (considering field of view, resolution, and pixel smearing) in the range of altitudes from 300 to 1000 km. The selected lens is a Fujinon HF25HA-1B fixed focal length lens, which will be focused to infinity. This lens has a primary diameter of 2.5 cm, resulting in a diffraction limit of about 7 arcseconds for red light. The lens will provide an angular field of view of 14.6° x 10.9° (crosstrack by downtrack), with a pixel width of 38 arcseconds. This field of view is larger than microbolometer field of view, allowing the visible camera to provide a wider context for the thermal images.

As with the microbolometer, the expected amount of pixel smearing was calculated. At an altitude of 500 km, the image footprint will be 127 x 95 km, giving each pixel a width of 92 m. For a shutter speed faster than 0.01 s and at an altitude of 500 km, the satellite's ground track will shift by less than one pixel, which is negligible. At higher altitudes, pixel smearing will be decreased further, but resolution will also decrease.

IMAGE PROCESSING ALGORITHMS

Two types of image processing algorithms will detect thermal features onboard the R^3 satellite; the first is known as the blobber algorithm and the second is based on edge detection theory.

The blobber algorithm detects contiguous areas whose pixels belong to a specified intensity range. A contiguous area, or blob, is defined as one for which each pixel has at least one of the eight neighboring pixels also belonging to the same area. The intensity range is defined based on the thermal signature of the feature to be detected. Scanning the image, the pixels that belong to the intensity range are differentiated from the ones that do not. Next, contiguous areas, or blobs, are extracted, while isolated pixels within the intensity threshold are discarded. The algorithm then calculates the area of each detected blob and selects the blobs that should be kept based on the expected area of the features to be detected. Finally, the algorithm provides the option to calculate the precise coordinates of the center of brightness of the detected feature.

The second type of algorithm is based on edge detection theory, which involves superposing the image with a "mask" containing weight coefficients. The output image is calculated by multiplying the pixel value by the mask coefficient. An illustration of this process is given in Equation 1 and Figure 2 below, where a_{ij} are the original image pixels, m_{ij} are the mask weight coefficients, and b_{ij} are the output image pixels.

$$\begin{aligned} b_{22} &= (a_{11} \times m_{11}) + (a_{12} \times m_{12}) + (a_{13} \times m_{13}) + (a_{21} \times m_{21}) + (a_{22} \times m_{22}) \\ &\quad + (a_{23} \times m_{23}) + (a_{31} \times m_{31}) + (a_{32} \times m_{32}) + (a_{33} \times m_{33}) \end{aligned} \tag{1}$$

a_{11}	a_{12}	a_{13}	...	a_{1n}
a_{21}	a_{22}	a_{23}	...	a_{2n}
a_{31}	a_{32}	a_{33}	...	a_{3n}

m_{11}	m_{12}	m_{13}
m_{21}	m_{22}	m_{23}
m_{31}	m_{32}	m_{33}

b_{11}	b_{12}	b_{13}	...	b_{1n}
b_{21}	b_{22}	b_{23}	...	b_{2n}
b_{31}	b_{32}	b_{33}	...	b_{3n}

Figure 2. Illustration of the edge detection algorithm process.

The algorithms can be used separately or together. By itself, the blobber algorithm can detect features of interest, such as wild fires. With the edge detection algorithm, it can perform detection of eddies and Gulf Stream tracking, useful for environmental purposes as well as military applications.

ORBIT LIFETIME STUDY

In order to define potential orbits that would be acceptable for the R^3 mission, the R^3 team first had to determine the range of acceptable initial orbit altitudes, which is limited due to the direct relationship between initial altitude and orbit lifetime. The lower end of the altitude range is bounded by the length of the baseline science mission, which consists of the mission phases from startup through normal operations (approximately 192 days, or 0.52 years). The upper end of the altitude range is bounded by the deorbit requirement imposed by the UNP User's Guide, which states that the satellite must deorbit within 25 years of the end of its mission. For the R^3 mission, this means the satellite must deorbit after completion of the baseline science mission plus 25 years (approximately 9323 days, or 25.52 years).

To ensure that these constraints would be met, an orbit lifetime study was conducted using Program to Optimize Simulated Trajectories (POST II). Two end-state altitudes were considered. First, an end-of-usable-life altitude of 200 km was selected; when this altitude is reached, the "End of Mission" mission phase will commence, including end-of-mission safing. Second, a disposal altitude of 78 km was defined; at this altitude the satellite's aluminum structure will break up in the Earth's atmosphere.

The orbit lifetime study using POST II considered circular orbits at various altitudes, including the upper and lower limits of the International Space Station (ISS) altitude range (278-460 km). The orbit lifetime until the end-of-usable-life altitude (200 km) and until the disposal altitude (78 km) is reported in Table 5. The satellite always reached the disposal altitude within three days of reaching the end-of-usable-life altitude.

Table 5. Orbit lifetime until satellite reaches end-of-usable-life altitude (200 km) and disposal altitude (78 km).

Initial Altitude (km)	**Orbit Lifetime (Until 200 km)**	**Orbit Lifetime (Until 78 km)**
250	5 days	8 days
278*	15 days	18 days
300	29 days	31 days
350	99 days	101 days
400	276 days	278 days
460*	2.2 years	2.3 years
500	4.4 years	4.4 years
550	10.2 years	10.2 years
600	23.4 years	23.4 years
650	52.4 years	52.4 years

*Upper and lower limits of ISS altitude range

Note that to achieve a six-month baseline science mission, a minimum orbit lifetime of 192 days is required, which corresponds to an initial altitude of roughly 382 km. To meet the deorbit requirement, a maximum orbit lifetime of 25.52 years is required, which corresponds to about 605 km altitude. Based on these figures, the R^3 team selected an altitude range of 300-600 km to be used for further mission analysis. While the lower limit of the altitude range precludes a six-month science mission, it adds flexibility to our mission by allowing the R^3 satellite to be launched with a wider variety of primary payloads, including most payloads travelling to the ISS.

INITIAL SCIENCE ORBIT

If selected by the University Nanosat Program, the R^3 satellite will launch as a secondary payload following the completion of the competition. Since the launch vehicle and latitude of the launch site will depend on the primary payload, they will remain unknown throughout the design phase. Thus, the orbital elements (e.g., periapsis altitude, eccentricity, inclination, and argument of periapsis) that describe the initial orbit in which the R^3 satellite will be placed cannot be determined explicitly.

A number of mission parameters and subsystems depend on the initial science orbit. Higher altitudes affect the performance of the visible and thermal imagers by decreasing resolution, increasing the image footprint size, and decreasing pixel smearing. If the orbit is eccentric, these imaging parameters will vary throughout the mission. Thus, periapsis altitude and eccentricity will influence the selection of appropriate imaging features. In addition, each of the four previously mentioned orbital elements affect the number of overflights of the Georgia Tech tracking station and the quality of the communication signal, which in turn determine the duration of ground communication opportunities and the data volume downlink capability. The latter of these parameters has a direct impact on mission success, since it determines the amount of science data that can be returned. Even the design of the tracking station depends on the expected orbit, since the ground receiving antenna must be able to sweep through the appropriate azimuth and elevation ranges at a sufficient rate to track the satellite.

Since the orbit is not precisely known but affects many mission design parameters, a design space exploration was performed to gain a better understanding of the impact of various orbits on the overall mission characteristics. A total of 48 orbits were considered, with orbital elements selected from the ranges presented in Table 6. These orbital element ranges are considered to be the most likely scenarios based on potential launch vehicle and launch site combinations. Note that only circular orbits were considered; this decision was based on feedback from UNP representatives and served to simplify the design space.

Table 6. Ranges of orbital elements considered in the orbit design space exploration.

Orbital Element	**Range**
Periapsis Altitude	300 – 600 km
Eccentricity	0.0
Inclination	34° – 90°
Argument of Periapsis	0° – 360°

Using Satellite Tool Kit (STK), the Georgia Tech tracking station and the R^3 satellite were modeled, and the 48 orbits being considered were simulated for a period of two weeks. The two-week time period was chosen to reflect the mission planning cycle (the length of time over which the orbit will be propagated for use in selecting imaging features) and was considered to be representative of the full six-month mission. A number of outputs were collected, and sample statistics were calculated to describe the distribution of the outputs across the 48 orbits. These statistics are tabulated in Table 7 below.

Table 7. Sample statistics describing the distribution of two-week output parameters across 48 potential orbits (where "overflights" refer to passes over the Georgia Tech tracking station).

Output Parameter	**Min**	**Max**	**Average**	**Standard Deviation**
Number of Overflights	18	62	37.5	14.8
Average Duration of Overflights (min)	2.4	5.5	3.8	0.9
Minimum Gap in Overflights (hrs)	1.5	11.3	5.1	4.2
Maximum Gap in Overflights (hrs)	12.3	36.0	20.4	7.2
Range (km)	309	1363	681	260
Azimuth (deg)	54.9	312.6	198.3	82.8
Elevation (deg)	20.9	83.0	46.8	18.8
Range Rate (km/s)	-0.19	0.33	0.001	0.11
Azimuth Rate (deg/s)	-3.87	4.88	-0.21	1.48
Elevation Rate (deg/s)	-0.37	0.55	0.004	0.13

DATA RETURN STRATEGY

A study was performed by the C&DH lead, the Mission Design lead, and the Telecom lead to determine the following:

1. The downlink capability of the R^3 spacecraft in terms of expected orbits and possible transmit data rates at each point on each orbit to maintain margin.
2. The desired R^3 mission architecture in terms of how frequently images are collected and how many images are sent to the ground.
3. The data volume these different mission architectures would produce.

Data Volume Downlink Capability

Beginning with the STK model discussed in the Initial Science Orbit section above, a study was conducted of the 48 orbits being considered, which were again simulated for a period of two weeks. During this two-week period, outputs were collected for each pass over the tracking station of each of the 48 orbits. These outputs were elevation angle, range, and time (i.e., duration of the communication window).

Previously, a link budget was developed using Microsoft Excel that used fixed parameters from selected representative (or expected worst case) orbits. However, the large set of orbits considered requires a more adaptable link budget that does not involve manual parameter input. A much more accurate expected downlink capability was therefore computed by converting the link budget into a number of computer-coded interrelated equations. The orbit data from STK (described in the Initial Science Orbit section) was then be set as the input into this link budget code to output the maximum possible data volume to be downlinked for a two-week period. This process was repeated for each of the 48 orbits being considered.

In a typical link budget, the link margin is calculated as a function of data rate, and the goal is to maximize the margin. The approach used by the R^3 team reversed this process. A link margin of 3 dB was set in accordance with standard JPL (Jet Propulsion Laboratory) practices, and the data rate (R) was calculated as a function of link margin and other parameters, as shown in Equation 1.

The intent of the R^3 team was to maximize the data rate, improving the amount of science data that could be transmitted.

$$R = P + L_G + L_l + G_t + L_s + L_a + G_r - 10\log(k) - 10\log(T_s) - \frac{E_b}{N_0} \quad (1)$$

The parameters in the above equation are defined as follows:

- P = transmitter power = 0 dB
- L_G = ground line loss = -5.9 dB
- L_l = transmitter line loss = -0.1 dB
- G_t = transmitter gain = 0 dB (worst case)
- L_s = space loss (calculated)
- L_a = transmission path loss (calculated)
- G_r = receiving antenna gain = 30 dB
- k = Boltzmann's constant
- T_s = system noise temperature = 6863 K
- E_b/N_0 = E_b/N_0 required + margin – implementation loss = 9.8 + 3.0 – 1.5 = 11.3 dB

It is important to note that the maximum data rate of the R^3 transceiver is 1 Mbps, so this was set as a ceiling in the code. It was found that, at this maximum data rate, not all of the 48 orbits being considered for the R^3 mission could maintain 3 dB link margin for every pass over the Georgia Tech tracking station. Thus, a variable data rate was implemented. The appropriate data rate was selected for a certain time increment by determining the maximum possible data rate that allowed the system to maintain a 3 dB margin for the duration of that time increment. Once the data rate was calculated, it was multiplied by the corresponding time increment to obtain the data volume. The data volumes for consecutive time increments were then summed over the total communication window to obtain the data volume downlink capability for a particular orbit.

Data Volume Production

Given the results of the above study, an analysis was performed to determine if the data volume downlink capability was sufficient for normal satellite operations and to determine how much science data could be downlinked from the satellite.

Several assumptions were made in order to assess the data volume produced. The analog to digital converter was assumed to produce 16 bit values, and all other incoming digital data was assumed to be 32 bits for each value. A default value for the frequency of telemetry data production (for downlink) was set to once every 60 seconds. This value may need to be higher for certain components, but it is assumed to be the default value for any components not explicitly specified. Finally, the RAW image format originating from the visible camera is assumed to be 16 bits per pixel.

An important aspect of communication links is the actual link utilization. This value will never reach 100% for single links which are capable of reliably transporting data because the data is either segmented to enable retransmission of corrupt data and/or it is interleaved with parities to enable a forward error correction. In the former case (which is the baseline for this design), data packet headers are needed to distinguish segments and in the latter, the parity data consumes a percentage of the data link. Therefore, the effective throughput is smaller than the data link throughput capability.

In order to calculate the estimated effective throughput, a lossless image compression of 40% was assumed. That is, the image data is reduced to 60% of its original size after the compression is applied. Also, a selective repeat-style protocol was assumed. This means that the receiver of data can request the sender to resend just the missing packets (determined via a timeout) or corrupted packets (determined via a checksum). Several other assumptions were made in order to calculate the effective throughput and are shown in Figure 3.

Assumptions			**Calculations**		
Bit Error Rate	0.00001	errors/bit	**Packet Total Size**	8392	bits
Packet Header Size	200	bits	**Packet Error Rate**	0.08392	errors/packet
Host Latency	0.001	s	**Quality Bits Sent / Window**	134217728	bits
Propagation Delay	0.005	s	**Bits Sent Per Window**	149033069	bits
Link Speed	500000	bps			
			Overhead Percentage	9.94%	
Packet Data Size	8192	bits			
Window Size	16384	packets	**Total Time to send window**	314.46	s
			Effective Bandwidth	426826	bps
Guidelines					
Overhead Optimal Packet Data Size	4477	bits			
Throughput Optimal Packet Data Size	8370	bits	**Effective Throughput Percentage**	**85%**	

Figure 3. Effective throughput calculation.

The effective throughput was found to be 85%, which means that any link data rate will need to be adjusted by this percentage to determine the amount of quality data that can be transmitted over that link.

The data volume production analysis involved first identifying all data-producing entities onboard the satellite, and then inputting the number of data bits produced and the frequency of data production for each data source. The telemetry data production for a two-week period was calculated for the normal mode of the satellite, since the satellite will produce the most data when operating in this mode.

The resulting data production information was meshed with the data volume downlink capability for the 48 orbits under consideration, and an analysis was performed to assess how many image pairs could be downlinked for a given orbit. Here, an image pair is defined as one thermal and one visible image (both compressed) of the same feature, plus radiation dosimeter data and telemetry.

Results

Once this analysis was complete, the R^3 team determined that the data volumes for the higher-inclination orbits were not sufficient to downlink even a single image pair in a two-week period. A second analysis was completed with the addition of a low-noise amplifier (LNA) on the ground receiving antenna, reducing the system noise temperature from 2863 K to 271 K. This assured that the data volume would be sufficiently high for all orbits considered. The sample statistics summarizing the distribution of data volume downlink capability across the 48 orbits are listed in Table 8 (without LNA) and Table 9 (with LNA).

Table 8. Data volume downlink capability sample statistics across the 48 orbits (without LNA).

	Data Volume Downlink Capability (Mb)
Minimum	178
Maximum	738
Average	354

Standard Deviation	199

Table 9. Data volume downlink capability sample statistics across the 48 orbits (with LNA).

	Data Volume Downlink Capability (Mb)
Minimum	569
Maximum	2363
Average	1136
Standard Deviation	639

The telemetry production for a two-week period was found to be 373 Mb, while an image pair was found to be about 15.25 Mb. Without the LNA, the communication system's data rate allowed at most 16 image pairs per two-week period to be downlinked, and only one third of the orbits were able to downlink all telemetry, radiation data, and at least one image pair. With the addition of the LNA, at least 120 image pairs could be downlinked per two-week period from any orbit examined, and at most 674 pairs. A plot of image pairs per two-week period versus orbit is shown in Figure 4 (without LNA) and Figure 5 (with LNA). The orbit labels list altitude (km), inclination (deg), and argument of periapsis (deg).

In these two figures, notice that the highest data volumes are achieved for orbits with inclinations of 34°; this is because the satellite's ground track spends more time near the latitude of the Georgia Tech tracking station than it does for higher-inclination orbits. Notice also that when the LNA is added (Figure 5), the number of image pairs for a given inclination increases with altitude in incremental stair-steps. This shows that the transceiver is reaching its maximum data rate of 1 Mbps (if it were not constrained by this ceiling on the data rate, the number of image pairs would be even higher). This trend is caused by the lower space loss due to the addition of the LNA, which allows the link to maintain the 3 dB margin at each altitude while still transmitting at a high data rate. Thus, since the data rate is fixed at 1 Mbps, the data volume returned becomes directly proportional to the amount of time spent over the ground station, which increases with altitude.

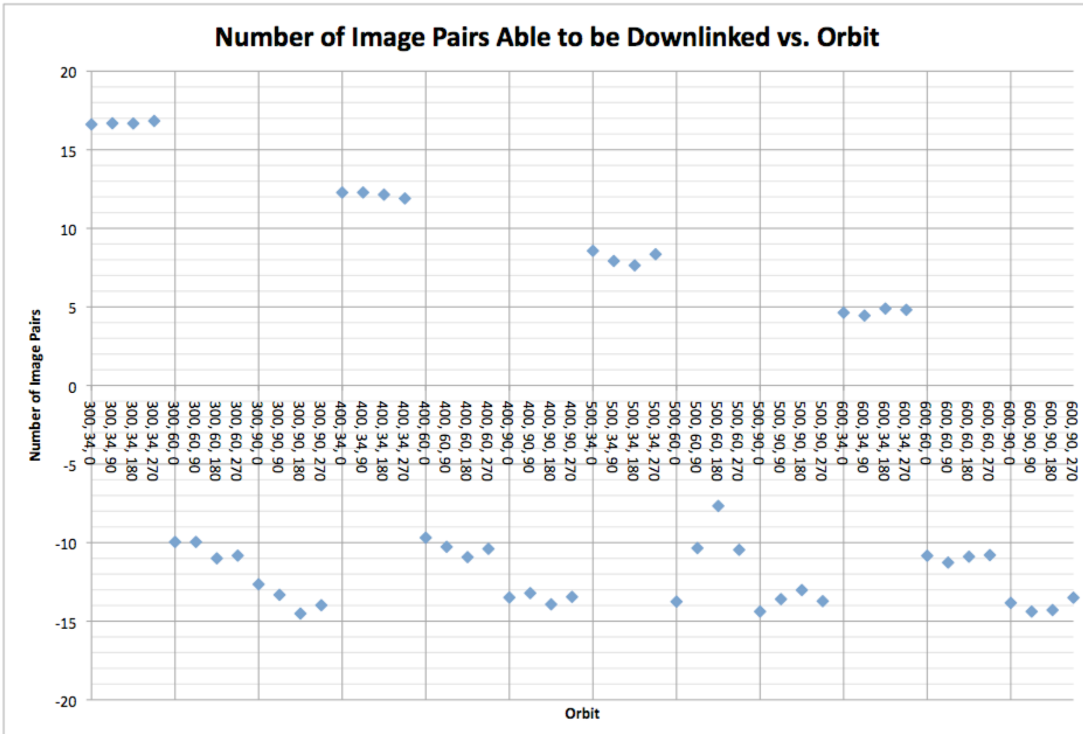

Figure 4. Number of image pairs able to be downlinked in two weeks vs. orbit (without LNA).

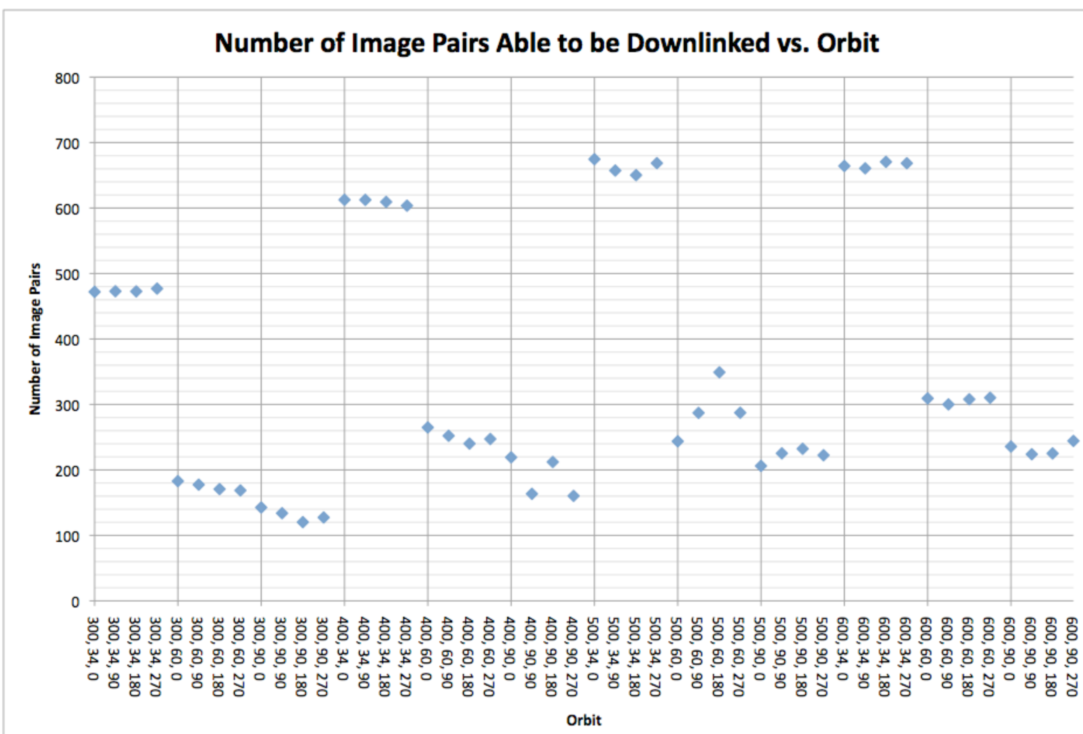

Figure 5. Number of image pairs able to be downlinked in two weeks vs. orbit (with LNA).